This article has been accepted for publication in a future issue of this journal, but has not been fully edited. Content may change prior to final publication. Citation information: DOI 10.1109/TWC.2021.3075099, IEEE Transactions on Wireless Communications



# Line-of-Sight Probability for mmWave-based UAV Communications in 3D Urban Grid Deployments

Margarita Gapeyenko, Dmitri Moltchanov, Sergey Andreev, and Robert W. Heath Jr.

***Abstract*—The network operators will soon be accommodating a new type of users: unmanned aerial vehicles (UAVs). 5G New Radio (NR) technology operating in the millimeter-wave (mmWave) frequency bands can support the emerging bandwidth-hungry applications facilitated by such aerial devices. To reliably integrate UAVs into the NR-based network infrastructure, new system models that capture the features of UAVs in urban environments are required. As city building blocks constitute one of the primary sources of blockage on the links from the UAV to its serving base station (BS), the corresponding line-of-sight (LoS) probability models are essential for accurate performance evaluation in realistic scenarios. We propose a LoS probability model in UAV communication setups over regular urban grid deployments, which is based on a Manhattan Poisson line process. Our approach captures different building height distributions as well as their dimensions and densities. Under certain characteristic distributions, closed-form expressions for the LoS probability are offered. Our numerical results demonstrate the importance of accounting for the building height distribution type as well as the orientation of the UAV with respect to its BS. By comparing our model with the standard ITU and 3GPP formulations, we establish that the latter provide an overly optimistic approximation for various deployments.**

***Index Terms*—3D LoS probability, urban grid deployment, mmWave radio, UAV communication, 5G NR technology**

## I. Introduction

According to recent studies, millimeter-wave (mmWave) communication promises to support connectivity between unmanned aerial vehicles (UAVs) and their serving radio infrastructure [1], [2]. With larger available bandwidths, mmWave transmission enables UAV-based applications and services that require high data rates, such as real-time video transfer, area surveillance, and many more. As mmWave bands are embraced by 5G New Radio (NR) access technology, the latter is expected to accommodate a new type of UAV users [3]–[5]. However, the incorporation of specific UAV features, such as their three-dimensional (3D) mobility, introduces further challenges and requires modifications to the existing channel models [6], [7].

One of the essential roadblocks for arranging seamless UAV support in mmWave-based 5G NR systems is the blockage of line-of-sight (LoS) radio propagation paths. As UAVs are envisioned to be utilized in city deployments [8], buildings constitute a major source of LoS blockage for the UAV to base station (BS) links [9]. The penetration losses on mmWave links occluded by a building may reach up to 40 dB [10], which can cause frequent and harmful service interruptions. As a result, characterizing the LoS blockage probability is a timely and important problem in the field.

The challenge of LoS blockage by buildings in urban deployments has been addressed in the literature, where several models were ratified by 3GPP and ITU-R [11], [12]. However, as we review in Section II, most of these earlier efforts consider fixed building heights and/or widths as well as randomized building layouts. These deployment parameters may significantly affect the resultant LoS probability, especially in urban grid scenarios. Moreover, some of the past models do not allow for simple closed-form solutions for the LoS probability that are suitable for further performance assessment of the prospective UAV deployments with system-level evaluations.

In this work, we develop an analytical model to derive the LoS probability for both fixed UAV locations and the cases where the UAVs are distributed uniformly over the BS coverage area. We consider a regular urban grid deployment of building blocks captured by a Manhattan Poisson line process (MPLP) having generally distributed building heights. For the fixed UAV location case, we produce a closed-form expression for the LoS probability under certain characteristic distributions of building heights. Our proposed model is capable of assessing the impact of urban grid deployment type on the LoS probability for the UAV to BS connections. Further, we systematically study the effects of the building heights and densities on the links between the UAV and its serving BS.

The main contributions of this work are the following.

- We propose a novel mathematical model that captures the essential details of 3D urban grid deployments to assess the existence of the LoS BS-to-UAV path. The developed model provides the LoS probability as a closed-form solution for a set of well-known building height distributions.
- Our performance evaluation campaign demonstrates that the LoS probability is highly sensitive to the (i) type of the urban grid deployment, (ii) form of the building height distribution, and (iii) UAV location with respect to the BS.
- Our comparison of the proposed model with the existing standardized formulations (e.g., those by 3GPP and ITU-R) indicates that the latter offer an overly optimistic approximation for the UAV LoS probability for a range of various deployments.

The rest of this text is organized as follows. In Section II, we provide a brief account of the related studies. Further,

M. Gapeyenko, D. Moltchanov, and S. Andreev are with Tampere University, Tampere, Finland (e-mail: firstname.lastname@tuni.fi)

R. W. Heath Jr. is with North Carolina State University, Raleigh NC (e-mail: rwheathjr@ncsu.edu)

This work was supported in part by the Academy of Finland (projects RADIANT and IDEA-MILL), JAES Foundation (project STREAM) and in part by the National Science Foundation under Grant No. ECCS-1711702 and CNS-1731658.

in Section III, our system model is outlined together with its main components. In Section IV, the respective analysis method is developed. We study the effects of the key system parameters on the UAV LoS blockage probability in Section V. The conclusions are offered in the last section.

## II. Related Work

In this section, we provide a literature review related to the blockage in general. We then give a comprehensive description of the LoS blockage models available to the academia and standardization bodies.

### A. Blockage Modeling

According to the IMT-2020 requirements [13], the channel models for the bands of above 6 GHz should have accurate 3D space-time characteristics in LoS and non-LoS (nLoS) conditions. Different types of blockage may transition the channel state from LoS to nLoS, namely: (i) self-body blockage, e.g., head of a user; (ii) small-scale blockage, e.g., vehicle or human body; and (iii) large-scale blockage, e.g., buildings.

In [14], the study delivered a model characterizing self-body blockage via a cone blockage approach. In [15], the authors proposed a method to calculate the probability of blockage caused by human bodies, where humans are distributed uniformly over the area. Application of stochastic geometry tools allowed to capture more comprehensive human-body blockage scenarios. For example, in [16], the proposed model simultaneously accounted for link blockage, transmission directivity, and vertical or horizontal directionality of transmit and receive antennas in mmWave UAV-to-ground communication scenarios. In [17], a coverage analysis was offered, while in [18], an overview of mathematical models for mmWave system modeling was provided.

There are two inherent properties of the reviewed models that allow for in-depth analysis: (i) distance between the BS and the user equipment (UE) is assumed to be much larger as compared to the dimensions of blockers and (ii) humans are distributed irregularly over the landscape. The latter property permits to utilize purely random models of UE locations, such as Poisson Point Process (PPP), while the former one does not force to count the exact number of blockers that may or may not occlude the LoS propagation path. However, these two properties do not hold for large-scale blockage. Below, we conduct a review of the existing LoS probability models that consider large-scale blockage and complete this section by indicating the gap that the proposed model can fill in.

### B. Large-Scale Blockage

There has been extensive work to estimate, analytically evaluate, or otherwise compute the LoS probability due to blockage by buildings. The research back from 1984 [19] proposed a mathematical formulation to derive the LoS probability in built-up areas for a receiver (Rx) to transmitter (Tx) pair. The proposed framework [19] relied on an analysis of the mean free path of moving particles in randomly distributed targets. The resultant LoS probability was calculated for the scenario where buildings are located along the $X$-axis between the Tx and the Rx, and under exponentially distributed building heights.

Further, in [20], the scenario considered a link between a ground user and a satellite. That study addressed the blockage arising from the buildings directly adjacent to the Rx because of the high altitudes of satellites. Hence, the derivation of the LoS probability was reduced to an integration of the building heights. The work in [21] considered the Fresnel zone to derive the LoS probability. For this purpose, a single knife-edge diffraction model was employed to identify the radius of the Fresnel zone and thus characterize the LoS probability.

The recent studies of terrestrial mmWave users actively considered the LoS probability due to its significant role in mmWave communication scenarios [18]. Particularly, the research in [22] contributed an analytical framework to establish the LoS probability for Tx to Rx links in an irregular deployment of buildings. The latter was represented as random-sized rectangles with the centers forming a PPP on a plane. The proposed approach argued for a reasonable approximation of the LoS probability in the scenarios where deployment is irregular, e.g., a university campus.

Later, the research in [23] contributed the LoS probability for air-to-everything links in a scenario with randomly distributed screens by following a similar approach as in [22]. The screens were representative of buildings with their height disregarded in the derivations. To further simplify the LoS modeling and provide a closed-form expression for the LoS probability, the work in [24] demonstrated the so-called LoS ball model. Accordingly, there is a circular area of a certain radius around the BS, where there is LoS with probability 1. Otherwise, there is link blockage for the Rx located outside of this radius.

The study in [25] proposed a frequency-dependent LoS probability model for a scenario with randomly-dropped cuboid buildings and uniformly-distributed building heights. That work also considered the first Fresnel zone and delivered the LoS probability in its integral form. Closed-form solutions were obtained for a number of special cases of interest including the situation where there is no height difference between the Tx and the Rx.

Not limited to irregular urban deployments, a number of studies addressed regular urban grids. In [26], the derived framework captured an urban grid with the MPLP wherein its lines represented the streets. Due to the features of the considered setup, where the user height was assumed to be shorter than the building height, the model imposed LoS conditions whenever a user was located on the street where the BS was deployed. However, this approach is not directly applicable to the UAV users as their altitudes of flight are comparable to the heights of buildings and cannot be ignored.

In [27], the authors contributed system-level simulation results for LTE and mmWave-based systems that support UAVs. That study was based upon real-world data from the city of Gent. Particularly, it reported the LoS probability between the terrestrial BSs and the UAV as a function of the UAV height derived from simulation data. The research in [28] proposed a method for deriving the LoS probability based on a

This article has been accepted for publication in a future issue of this journal, but has not been fully edited. Content may change prior to final publication. Citation information: DOI 10.1109/TWC.2021.3075099, IEEE Transactions on Wireless Communications



point cloud collected with a scan laser, where it was checked whether any point fell into the Fresnel zone of a BS-to-UE link. The methodology in question was applied to both open-square and shopping-mall scenarios for gathering the data and fitting them into an exponential LoS probability model.

A large-scale measurement campaign for the LoS probability was performed in [29] by using a ray-tracing approach. Similarly to [28], the obtained statistical data were fitted to the model. A limitation of these past studies is in the amounts of time required to conduct measurement campaigns, ray-tracing studies, or system-level simulations on the city-wide scales and with varying parameters, such as BS and building heights, etc.

### C. UAV LoS Modeling by 3GPP and ITU-R

ITU-R and 3GPP also considered an urban grid deployment as part of their efforts. Particularly, ITU-R P.1410 [12] addressed the frequency range of 20 to 50 GHz. The LoS probability was defined as $\mathbb{P}^{\text{ITU}}_{\text{LoS}}(r, h_{\text{T}}, h_{\text{R}}, \alpha, \beta, \gamma)$, which is the probability that the Tx-to-Rx link is not occluded by a building. The input parameter $r$ is the two-dimensional (2D) distance in kilometers between the Tx and the Rx, $h_{\text{T}}$ and $h_{\text{R}}$ are the Tx and Rx heights, respectively. The value of $\alpha$ is the fraction of the area covered by buildings to the total area, $\beta$ is the average number of buildings per unit area, and $\gamma$ is a height distribution parameter.

To simplify the notation, we further employ $\mathbb{P}^{\text{ITU}}_{\text{LoS}}$ as the ITU LoS probability, which is given as

$$\mathbb{P}^{\text{ITU}}_{\text{LoS}} = \prod_{n=0}^{m} \left( 1 - \exp\left( \frac{(h_{\text{T}} - \frac{(n+\frac{1}{2})(h_{\text{T}}-h_{\text{R}})}{m+1})^2}{2\gamma^2} \right) \right), \quad (1)$$

where $m = \lfloor r\sqrt{(\alpha\beta)} \rfloor - 1$ is the number of buildings in-between Tx and Rx. The work in [30] considered this model for the air-to-ground LoS probability modeling. One of the limitations of this formulation is that it assumes the building bases to be perpendicular to the LoS projection between the Rx and the Tx onto $\Re^2$. Even though the model accounts for different mean heights of Tx and Rx, it captures neither alternative building height distributions nor the LoS angle of departure (AoD). Finally, the output of this modeling is only available in the product-form, which limits its applicability.

To broadly characterize the UAV-based scenarios, 3GPP in TR 36.777 [11] proposed a LoS probability model for the link between the UAV and the BS. It distinguishes various deployment types by delivering separate dedicated solutions. The structure of this model is different for various heights of the BS and the UAV. Below, we provide an example for the UMi street canyon LoS model $\mathbb{P}^{\text{3GPP}}_{\text{LoS}}(\ell_{\text{2D}}, h_{\text{R}})$, which is applicable for $h_{\text{T}} = 10\,\text{m}$ and the UAV heights in the range of $22.5\,\text{m} < h_{\text{R}} < 300\,\text{m}$. The input parameter $\ell_{\text{2D}}$ is the 2D distance in meters between the UAV and the BS.

We further employ $\mathbb{P}^{\text{3GPP}}_{\text{LoS}}$ as the 3GPP LoS probability that is defined as follows[1]

$$\mathbb{P}^{\text{3GPP}}_{\text{LoS}} = \begin{cases} 1, & \ell_{\text{2D}} \le d, \\ \frac{d}{\ell_{\text{2D}}} + \left[1 - \frac{d}{\ell_{\text{2D}}}\right] \exp\left[\frac{-\ell_{\text{2D}}}{p_1}\right], & \ell_{\text{2D}} > d, \end{cases} \quad (2)$$

where the variables $p_1$ and $d$ are given as

$$\begin{aligned} p_1 &= 233.98 \log_{10}(h_{\text{R}}) - 0.95, \\ d &= \max(294.05 \log_{10}(h_{\text{R}}) - 432.94,\ 18). \end{aligned} \quad (3)$$

The precomputed parameters of the 3GPP LoS model do not permit to alter the deployment dimensions, such as building heights or densities. Furthermore, 3GPP provided the LoS model for a fixed BS height.

To summarize, when considering the UAV-to-BS operation in typical urban deployments, one cannot assume purely stochastic deployments of blockers as cities typically follow semi-regular street layouts. Moreover, the sizes of blockers are then comparable to the lengths of the propagation paths. Hence, one needs to explicitly consider each potential blocker and its position with respect to the LoS path. Finally, as the UAV height is comparable to the heights of buildings (in contrast to the terrestrial users), the latter cannot be disregarded in the LoS blockage modeling.

Despite several studies completed to date, there are no LoS probability models that simultaneously capture the features of a regular urban grid deployment, the planar urban geometry, and the building height distribution. As many of the civil UAV-based applications, such as video monitoring and package delivery, are more relevant in urban deployments, the intended LoS link blockage analysis in the corresponding environment becomes essential.

Having an accurate LoS probability model as part of system-level analysis allows to calculate the metrics of interest more carefully and thus assess the operation of a UAV-ready network. The system-level simulation times in UAV-centric scenarios may be reduced dramatically by avoiding exact modeling of the city deployment and instead employing analytical LoS probability values. In what follows, we propose a new LoS model that captures the said parameters, assess their effects, and compare the results against those for the formulations ratified by 3GPP and ITU-R.

## III. System Model

In this section, we introduce the considered urban grid deployment. We then specify additional assumptions on the locations of the communicating entities and define the metrics of interest. The main parameters are collected in Table I.

### A. Urban Grid Layout

We consider an urban grid setup illustrated in Fig. 1. It assumes that the mean side of a building block is equal to $\mu_{\text{b}}$ and the mean street width is $\mu_{\text{s}}$. To capture a Manhattan-type urban grid deployment, we utilize a commonly-employed MPLP [26] as shown in Fig. 1(b). This process is specified by

[1]For different BS heights, $h_{\text{T}}$, 35 m for RMa-AV, 25 m for UMa-AV, refer to Table B-1, TR 36.777. For $h_{\text{R}}$ below 22.5 m, the UMi model in Table 7.4.2-1 of TR 38.901 becomes applicable.

This article has been accepted for publication in a future issue of this journal, but has not been fully edited. Content may change prior to final publication. Citation information: DOI 10.1109/TWC.2021.3075099, IEEE Transactions on Wireless Communications



two one-dimensional (1D) homogeneous PPPs along the $X$- and $Y$-axis with the intensity $\lambda = 1/(\mu_\mathrm{b} + \mu_\mathrm{s})$ and the origin at point $O$. The points generated by the PPPs are the origins of the streets displayed as parallel straight lines in Fig. 1(b).

We assume that the line segment between two neighboring points along the $X$- and $Y$-axis contains the side of a building block (hereinafter referred to as "block") in the proportion of $\mu_\mathrm{b}/(\mu_\mathrm{b} + \mu_\mathrm{s})$, while the remainder is the street. As demonstrated in Fig. 1(b), the resultant rectangles represent buildings. They act as potential blockers for the LoS path between the BS and the UAV. The height of each block is a random variable (RV) $H_\mathrm{B}$ with the probability density function (pdf) $f_{H_\mathrm{B}}(h)$ and the cumulative distribution function (CDF) $F_{H_\mathrm{B}}(h)$.

### B. Network Deployment

Further, we consider the locations of the BS and the UAV in our urban grid layout as illustrated in Fig. 1(a). We assume that the BS is deployed along the street named a *typical street*. The location ground point of the BS is point $T$ and the height is $h_\mathrm{T}$. The UAV is placed at point $R$ and at height $h_\mathrm{R}$. We assume that the UAVs cannot be located inside buildings. The building always remains below the UAV in the case where their 2D positions coincide. There are two commonly considered BS locations in urban grid deployments, which are studied in our work [31]:

- The BS is placed at the intersection of two perpendicular typical streets with a constant width of $w_\mathrm{h}$ and $w_\mathrm{v}$. In this scenario, the origin of the urban grid is located $K_\mathrm{h} w_\mathrm{h}$ and $K_\mathrm{v} w_\mathrm{v}$ away from the BS position as depicted in Fig. 2(a). The coefficients $K_\mathrm{h}$ and $K_\mathrm{v}$ in the range of $(0, 1)$ represent the relative position of the BS along the typical street, e.g., $K_\mathrm{h} = K_\mathrm{v} = 0.5$ refers to the BS located at the center of the intersection.
- The BS is placed on the typical street with a constant width of $w_\mathrm{v}$. In this scenario, the origin of the urban grid is $K_\mathrm{v} w_\mathrm{v}$ away from the BS position as shown in Fig. 2(b).

TABLE I
SUMMARY OF NOTATION AND PARAMETERS

| Notation | Description |
|---|---|
| $h_\mathrm{T}$ | BS height |
| $h_\mathrm{R}$ | UAV height |
| $H_\mathrm{B}$ | Building block height |
| $f_{H_\mathrm{B}}(h)$ | pdf of building block heights |
| $F_{H_\mathrm{B}}(h)$ | CDF of building block heights |
| $\ell_\mathrm{2D}$ | 2D distance between BS and UAV |
| $\phi_\mathrm{D}$ | LoS AoD |
| $\lambda$ | Intensity of points along $X$- and $Y$-axis |
| $w_\mathrm{h}$, $w_\mathrm{v}$ | Width of horizontal and vertical typical streets |
| $K_\mathrm{h}$, $K_\mathrm{v}$ | BS position coefficients on horizontal/vertical streets |
| $h_\mathrm{m}^0$ | LoS height at the intersection point with the first contact side |
| $h_\mathrm{m}^x(x)$ | LoS height at the intersection point with the vertical sides |
| $h_\mathrm{m}^y(y)$ | LoS height at the intersection point with the horizontal sides |
| $x_0$, $l_\mathrm{x}$ | $x$-coordinates of the first two LoS projections on $X$-axis |
| $y_0$, $l_\mathrm{y}$ | $y$-coordinates of the first two LoS projections on $Y$-axis |
| $p_\mathrm{s}$ | Probability of UAV being located on a typical street |
| $R$ | Cell radius |
| $f_\Phi(\phi_\mathrm{D})$ | pdf of LoS AoD |
| $f_L(l_\mathrm{2D})$ | pdf of BS to UAV 2D distance |
| $\mathbb{P}_\mathrm{LoS}$ | LoS probability |
| $\mathbb{P}^*_\mathrm{LoS}$ | Area LoS probability |

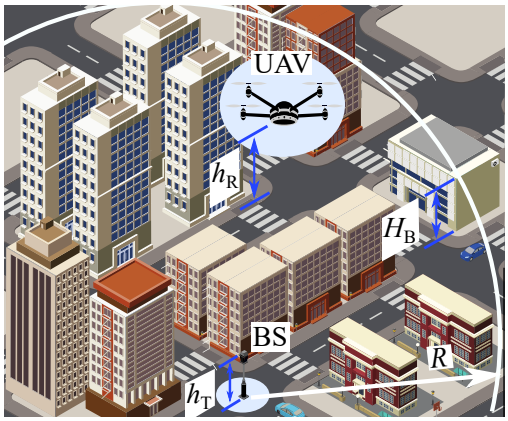


(a) 3D view of our scenario

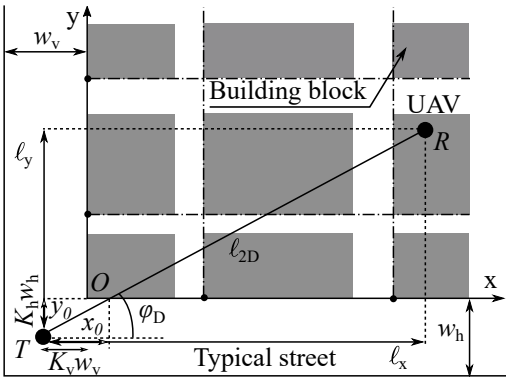


(b) 2D view of our scenario

Fig. 1. 3D and 2D urban grid snapshots for analytical modeling. BS base is located at point $T$. UAV having base projection $R$ onto 2D plane is separated by $\ell_\mathrm{2D}$ 2D distance from BS. Points along $X$- and $Y$-axis represent starting points of streets generated according to PPP with intensity $\lambda$.

We note that if $K_h = K_v = 0.5$, our scenario becomes fully symmetric. In this work, we also consider the BS coverage as a circle of radius $R$ on the plane, see Fig. 1.

### C. LoS Blockage

We proceed with the conditions leading to blockage of the BS-to-UAV link by buildings. Here, a LoS blockage decision is made based on an occlusion of the optical LoS. Therefore, a blockage occurs if at least one building that intersects the LoS is higher than the optical BS-to-UAV LoS path.

Note that the LoS projection on the 2D plane $TR$ can only cross the 2D projection of the left (perpendicular to the $X$-axis) and bottom (parallel to the $Y$-axis) sides of the blocks. We thus consider only the sides that actually affect the LoS blockage. We further refer to the side that is the first one to intersect with $TR$ as the *contact side*. The LoS 2D projection $TR$ can in fact intersect only one contact side of the block that it interacts with.

We continue with UAV placement in the considered deployment. For certainty, we consider the UAV located at any point of the first quadrant. Observe that such analysis is similar to that for other quadrants. Further, UAV location parameters $K_h = K_v = 0.5$ make our setup fully symmetric. We also require the height of the UAV to always remain above the

This article has been accepted for publication in a future issue of this journal, but has not been fully edited. Content may change prior to final publication. Citation information: DOI 10.1109/TWC.2021.3075099, IEEE Transactions on Wireless Communications



height of the block if its position coincides with this block. The latter forces the UAV to reside in the LoS or nLoS state depending on the blockage from buildings along the LoS path between the BS and the UAV. The 2D distance from the BS to the UAV is denoted as $\ell_{\text{2D}}$, while the LoS AoD is $\phi_{\text{D}}$ as displayed in Fig. 1(b).

### D. Metrics of Interest

We conclude with a description of two metrics of interest, which are considered in our mathematical modeling. To characterize communication between the UAV and the BS in different urban deployments, we first address the *LoS probability* parameter. To capture the UAV inside the BS coverage, we then calculate the *area LoS probability*.

**Definition 1.** *The LoS probability is the probability that the height of every building with its base intersecting the LoS link projection is lower than the height of the LoS link between the BS and the UAV at the point of their intersection.*

Therefore, for a fixed UAV location, we derive the LoS probability conditioned on the urban grid deployment, the UAV height, the UAV-to-BS separation distance, and the AoD value. This parameter of interest can be incorporated into further system-level analysis of UAV networks. Comprehensive performance evaluation of such setups aims at demonstrating the capability of wireless networks to accommodate UAV users.

**Definition 2.** *The area LoS probability is the probability that the LoS link between the UAV (distributed randomly and uniformly within the BS coverage of radius $R$) and the BS is not occluded by any building with its base intersecting the LoS link projection on a 2D plane.*

We evaluate the area LoS probability within the region of radius $R$, where $R$ can be selected, e.g., based on the BS density. The latter parameter of interest provides insights into whether the current BS deployment is sufficiently provisioned to support the UAVs. If the area LoS probability is low, one may adjust the inter-site distance between the BSs by reducing their coverage radius. Another option is to consider different BS heights for supporting aerial users.

## IV. Proposed Analysis

In this section, we derive the two metrics of interest based on the system model and the assumptions introduced above. Below, we briefly outline our approach and then proceed by calculating the UAV LoS probability and the area LoS probability.

### A. Methodology at Glance

To determine the LoS probability, $\mathbb{P}_{\text{LoS}}$, it is sufficient to establish the probability that the 2D projection of the LoS path, $TR$, does not intersect a block, whose height is higher than the LoS height at the point of intersection. We then need to determine all the contact sides of $TR$ by specifying the probability that the height of the building side at 2D distance of $x$ is lower than the height of LoS at $x$, $Pr\{H_{\text{B}} < h^x_{\text{m}}(x)\}$.

We continue with determining the number of intersections of $TR$ with the contact sides. Even though there is a number of sides for every line perpendicular to the $X$-axis, the $TR$ can in fact intersect only one of them. Therefore, the number of intersections of $TR$ with the contact sides perpendicular to the $X$-axis equals the number of points on the $X$-axis generated between the points $T$ and $R$. The same holds for the sides perpendicular to the $Y$-axis.

Hence, to determine the LoS probability, there is no need to iterate over all of the possible combinations of blocks. To preserve analytical tractability, we recall that the width of the street is significantly smaller than the width of the block side. Consequently, we assume that the LoS path always intersects the side of the block. In Section V, we numerically confirm that this simplification does not impact the results significantly.

After identifying the number of intersections of $TR$ with the contact sides, we consider the actual LoS probability. For an UAV to experience the LoS conditions, all the contact sides intersecting the LoS path need to be lower than the LoS height at the point of their intersection. Hence, to determine the effective density of points occluding the LoS path, one has to thin the PPP with the probability of side height being above

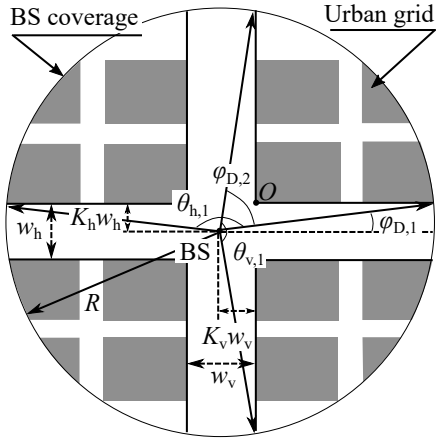


(a) BS located at intersection

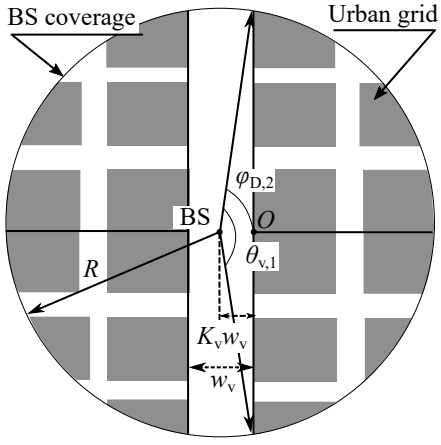


(b) BS located on street

Fig. 2. UAV is located randomly within BS coverage of radius $R$. Coefficients $K_h$ and $K_v$ in (0,1) determine BS location on typical streets. UAV located outside of typical streets has LoS AoD ($\phi_{\text{D},1}$, $\phi_{\text{D},2}$).

This article has been accepted for publication in a future issue of this journal, but has not been fully edited. Content may change prior to final publication. Citation information: DOI 10.1109/TWC.2021.3075099, IEEE Transactions on Wireless Communications



the LoS path, which leads to a non-homogeneous PPP.

Further, using the void probability of the resulting non-homogeneous PPP, one may determine the probability that there are no sides occluding the LoS path. The only exception to this procedure is that one also needs to account for the *first contact side*. The latter is the first side to be intersected by $TR$, which is located at a fixed distance from the BS position.

### B. Main Formulations

In this subsection, we derive our main results including the LoS probability and the area LoS probability.

**Proposition 1.** *The LoS probability, $\mathbb{P}_{LoS}(\ell_{2D},\phi_D)$, for the general distribution of building heights is given below. The expression employs $F_{H_B}(h)$ as the CDF of the block heights. $F_{H_B}\big(h^0_m(\ell_{2D},\phi_D)\big)$ is the probability that the first contact side height is lower than the LoS height, $h^0_m(\ell_{2D},\phi_D)$, at the point of their intersection.*

*$F_{H_B}\big(h^x_m(x,\ell_{2D},\phi_D)\big)$ and $F_{H_B}\big(h^y_m(y,\ell_{2D},\phi_D)\big)$ are the probabilities that the sides perpendicular to the $X$- and $Y$-axis are lower than the LoS heights, $h^x_m(x,\ell_{2D},\phi_D)$ and $h^y_m(y,\ell_{2D},\phi_D)$, at the point of their intersection, respectively.*

$$\mathbb{P}_{LoS}(\ell_{2D},\phi_D)=F_{H_B}\big(h^0_m(\ell_{2D},\phi_D)\big)\times \exp\left(-\lambda\int_{x_0}^{\ell_x}\Big[1-F_{H_B}\big(h^x_m(x,\ell_{2D},\phi_D)\big)\Big]dx-\lambda\int_{y_0}^{\ell_y}\Big[1-F_{H_B}\big(h^y_m(y,\ell_{2D},\phi_D)\big)\Big]dy\right). \quad (7)$$

*Proof.* First, we determine the distances from the point $T$ to the first and the second endpoints of the $TR$ projection on the $X$- and $Y$-axis, $x_0$, $\ell_{\rm x}$ and $y_0$, $\ell_{\rm y}$ as illustrated in Fig. 1(b) and is given below. These expressions contain the parameters $K_{\rm v}$ and $K_{\rm h}$, which are the coefficients related to the position of the BS on the typical vertical and horizontal streets, $w_{\rm v}$ and $w_{\rm h}$ that are the widths of such streets, and $\phi_{\rm D}$ as the LoS AoD.

$$\begin{aligned} x_0&=\max\big(K_{\rm v}w_{\rm v},K_{\rm h}w_{\rm h}\cot(\phi_{\rm D})\big),\\ \ell_{\rm x}&=\ell_{\rm 2D}\cos(\phi_{\rm D}),\\ y_0&=\max\big(K_{\rm h}w_{\rm h},K_{\rm v}w_{\rm v}\tan(\phi_{\rm D})\big),\\ \ell_{\rm y}&=\ell_{\rm 2D}\sin(\phi_{\rm D}). \end{aligned} \quad (8)$$

To derive the CDF $F_{H_{\rm B}}\big(h^x_{\rm m}(x,\ell_{\rm 2D},\phi_{\rm D})\big)$, one has to obtain the LoS height at the points of intersection with the sides perpendicular to the $X$-axis as a function of the 2D $TR$ projection on the $X$-axis, $x$. From the model geometry, the latter is calculated as

$$h^x_{\rm m}(x,\ell_{\rm 2D},\phi_{\rm D})=\frac{x(h_{\rm R}-h_{\rm T})+h_{\rm T}\ell_{\rm 2D}\cos(\phi_{\rm D})}{\ell_{\rm 2D}\cos(\phi_{\rm D})}. \quad (9)$$

Similarly, to find the CDF $F_{H_{\rm B}}\big(h^y_{\rm m}(y,\ell_{\rm 2D},\phi_{\rm D})\big)$, we establish the LoS height at the points of intersection with the sides that are perpendicular to the $Y$-axis as a function of the 2D $TR$ projection on the $Y$-axis, $y$ as

$$h^y_{\rm m}(y,\ell_{\rm 2D},\phi_{\rm D})=\frac{y(h_{\rm R}-h_{\rm T})+h_{\rm T}\ell_{\rm 2D}\sin(\phi_{\rm D})}{\ell_{\rm 2D}\sin(\phi_{\rm D})}. \quad (10)$$

The LoS height at the point of intersection with the first contact side for the CDF $F_{H_{\rm B}}\big(h^0_{\rm m}(\ell_{\rm 2D},\phi_{\rm D})\big)$ is provided below as

$$h^0_{\rm m}(\ell_{\rm 2D},\phi_{\rm D})=\frac{x_0(h_{\rm R}-h_{\rm T})}{\ell_{\rm 2D}\cos(\phi_{\rm D})}+h_{\rm T}. \quad (11)$$

Recalling the PPP properties [32], the probability that there are no sides perpendicular to the $X$-axis, which are higher than the LoS at the point of their intersection is derived by using the void probability of the thinned PPP, i.e.,

$$p^{(x)}_{\rm nB}(\ell_{\rm 2D},\phi_{\rm D})=\exp\left[-\lambda\int_{x_0}^{\ell_{\rm x}}\Big(1-F_{H_{\rm B}}\big(h^x_{\rm m}(x,\ell_{\rm 2D},\phi_{\rm D})\big)\Big){\rm d}x\right]. \quad (12)$$

Similarly, the probability that there are no sides perpendicular to the $Y$-axis, which are higher than the LoS, is given by

$$p^{(y)}_{\rm nB}(\ell_{\rm 2D},\phi_{\rm D})=\exp\left[-\lambda\int_{y_0}^{\ell_{\rm y}}\Big(1-F_{H_{\rm B}}\big(h^y_{\rm m}(y,\ell_{\rm 2D},\phi_{\rm D})\big)\Big){\rm d}y\right]. \quad (13)$$

The probability that the first contact side does not occlude the LoS is readily available by using the block height distribution in the form

$$p^{(0)}_{\rm nB}(\ell_{\rm 2D},\phi_{\rm D})=F_{H_{\rm B}}\big(h^0_{\rm m}(\ell_{\rm 2D},\phi_{\rm D})\big). \quad (14)$$

Since vertical and horizontal block and street deployments are independent from each other, the LoS probability is provided by a direct product of (12)-(14) as in (7). □

We now formulate three important corollaries that offer closed-form solutions for the LoS probability under three block height distributions that are widely used in the literature: uniform [33], exponential [19], and Rayleigh [12], [20]. These results are available via direct integration of (7).

**Corollary 1.** *For the uniformly distributed block heights $H_B\sim\mathcal{U}(h_1,h_2)$, the LoS probability is provided by*

$$\mathbb{P}_{LoS}(\ell_{2D},\phi_D)=\frac{h^0_m(\ell_{2D},\phi_D)-h_1}{h_2-h_1}\times \exp\left(-\lambda\int_{x_0}^{\ell_x}\Big[1-\frac{h^x_m(x,\ell_{2D},\phi_D)-h_1}{h_2-h_1}\Big]dx-\lambda\int_{y_0}^{\ell_y}\Big[1-\frac{h^y_m(y,\ell_{2D},\phi_D)-h_1}{h_2-h_1}\Big]dy\right), \quad (15)$$

*which leads to a closed-form solution in (4).*

**Corollary 2.** *For the exponentially distributed block heights $H_B\sim\exp(\lambda_B)$, the LoS probability is provided by*

$$\mathbb{P}_{LoS}(\ell_{2D},\phi_D)=\Big(1-\exp\big(-h^0_m(\ell_{2D},\phi_D)\lambda_B\big)\Big)\times \exp\left(-\lambda\int_{x_0}^{\ell_x}\exp\big(-h^x_m(x,\ell_{2D},\phi_D)\lambda_B\big)dx-\lambda\int_{y_0}^{\ell_y}\exp\big(-h^y_m(y,\ell_{2D},\phi_D)\lambda_B\big)dy\right), \quad (16)$$

This article has been accepted for publication in a future issue of this journal, but has not been fully edited. Content may change prior to final publication. Citation information: DOI 10.1109/TWC.2021.3075099, IEEE Transactions on Wireless Communications



$$\mathbb{P}_{\text{LoS}}(\ell_{\text{2D}},\phi_{\text{D}}) = \frac{h_{\text{m}}^0 - h_1}{h_2 - h_1} \times \exp\left(\frac{(h_2-h_{\text{T}})\big(-\lambda(\ell_{\text{x}}-x_0)-\lambda(\ell_{\text{y}}-y_0)\big)}{h_2-h_1} + \frac{\lambda(\ell_{\text{x}}^2-x_0^2)(h_{\text{R}}-h_{\text{T}})}{2\ell_{\text{2D}}(h_2-h_1)\cos(\phi_{\text{D}})} + \frac{\lambda(\ell_{\text{y}}^2-y_0^2)(h_{\text{R}}-h_{\text{T}})}{2\ell_{\text{2D}}(h_2-h_1)\sin(\phi_{\text{D}})}\right). \quad (4)$$

$$\mathbb{P}_{\text{LoS}}(\ell_{\text{2D}},\phi_{\text{D}}) = \left[1-\exp(-h_{\text{m}}^0\lambda_{\text{B}})\right]\exp\left(\frac{\lambda\ell_{\text{2D}}\exp(-\lambda_{\text{B}}h_{\text{T}})\cos(\phi_{\text{D}})}{\lambda_{\text{B}}(h_{\text{R}}-h_{\text{T}})}\left(\exp\left[\frac{-\lambda_{\text{B}}\ell_{\text{x}}(h_{\text{R}}-h_{\text{T}})}{\ell_{\text{2D}}\cos(\phi_{\text{D}})}\right] - \exp\left[\frac{-\lambda_{\text{B}}x_0(h_{\text{R}}-h_{\text{T}})}{\ell_{\text{2D}}\cos(\phi_{\text{D}})}\right]\right) + \frac{\lambda d_{\text{2D}}\exp(-\lambda_{\text{B}}h_{\text{T}})\sin(\phi_{\text{D}})}{\lambda_{\text{B}}(h_{\text{R}}-h_{\text{T}})}\left(\exp\left[\frac{-\lambda_{\text{B}}\ell_{\text{y}}(h_{\text{R}}-h_{\text{T}})}{\ell_{\text{2D}}\sin(\phi_{\text{D}})}\right] - \exp\left[\frac{-\lambda_{\text{B}}y_0(h_{\text{R}}-h_{\text{T}})}{\ell_{\text{2D}}\sin(\phi_{\text{D}})}\right]\right)\right). \quad (5)$$

$$\mathbb{P}_{\text{LoS}}(\ell_{\text{2D}},\phi_{\text{D}}) = \left(1-\exp\Big(-\frac{(h_{\text{m}}^0)^2}{2\sigma^2}\Big)\right)\times \exp\left(\frac{-\lambda\ell_{\text{2D}}\cos(\phi_{\text{D}})\sigma\sqrt{\pi}\Big(\exp\Big(\frac{h_{\text{T}}^2\sigma^2-h_{\text{T}}^2}{2\sigma^2}\Big)\Big)\Big(\text{erf}\Big(\frac{(h_{\text{R}}-h_{\text{T}})\ell_{\text{x}}+h_{\text{T}}\ell_{\text{2D}}\cos(\phi_{\text{D}})\sigma}{\sqrt{2}\ell_{\text{2D}}\cos(\phi_{\text{D}})\sigma}\Big) - \text{erf}\Big(\frac{(h_{\text{R}}-h_{\text{T}})x_0+h_{\text{T}}\ell_{\text{2D}}\cos(\phi_{\text{D}})\sigma}{\sqrt{2}\ell_{\text{2D}}\cos(\phi_{\text{D}})\sigma}\Big)\Big)}{\sqrt{2}(h_{\text{R}}-h_{\text{T}})} + \frac{-\lambda\ell_{\text{2D}}\sin(\phi_{\text{D}})\sigma\sqrt{\pi}\Big(\exp\Big(\frac{h_{\text{T}}^2\sigma^2-h_{\text{T}}^2}{2\sigma^2}\Big)\Big)\Big(\text{erf}\Big(\frac{(h_{\text{R}}-h_{\text{T}})\ell_{\text{y}}+h_{\text{T}}\ell_{\text{2D}}\sin(\phi_{\text{D}})\sigma}{\sqrt{2}\ell_{\text{2D}}\sin(\phi_{\text{D}})\sigma}\Big) - \text{erf}\Big(\frac{(h_{\text{R}}-h_{\text{T}})y_0+h_{\text{T}}\ell_{\text{2D}}\sin(\phi_{\text{D}})\sigma}{\sqrt{2}\ell_{\text{2D}}\sin(\phi_{\text{D}})\sigma}\Big)\Big)}{\sqrt{2}(h_{\text{R}}-h_{\text{T}})}\right). \quad (6)$$

*which leads to a closed-form solution in (5).*

**Corollary 3.** *For the Rayleigh distributed block heights $H_B \sim$ Rayleigh$(\sigma)$, the LoS probability is provided by*

$$\mathbb{P}_{LoS}(\ell_{2D},\phi_D) = \left[1-\exp\Big(-\frac{\big(h_m^0(\ell_{2D},\phi_D)\big)^2}{2\sigma^2}\Big)\right]\times \exp\left(-\lambda\int_{x_0}^{\ell_x}\left[\exp\Big(-\frac{\big(h_m^x(x,\ell_{2D},\phi_D)\big)^2}{2\sigma^2}\Big)\right]dx - \lambda\int_{y_0}^{\ell_y}\left[\exp\Big(-\frac{\big(h_m^y(y,\ell_{2D},\phi_D)\big)^2}{2\sigma^2}\Big)\right]dy\right), \quad (17)$$

*which leads to a closed-form solution in (6).*

We continue with a characterization of the area LoS probability for the UAV that is located randomly within the BS cell area as depicted in Fig. 2.

**Proposition 2.** *The area LoS probability, $\mathbb{P}_{LoS}^*$, for the UAV that is located randomly and uniformly within the BS coverage area having the radius of $R$ is given by*

$$\mathbb{P}_{LoS}^* = p_s + (1-p_s)\mathbb{P}_{LoS}, \quad (18)$$

*where $p_s$ is the probability that the UAV projection onto the ground plane is located along the typical street (with BS), while $\mathbb{P}_{LoS}$ is the LoS probability as the UAV is placed at any other point.*

*The derivation of $\mathbb{P}_{LoS}$ contains $f_\Phi(\phi_D) \sim \mathcal{U}(\phi_{D,1},\phi_{D,2})$, which is the pdf of the AoD. We define $f_L(\ell_{2D}) \sim \mathcal{U}(x_0/\cos(\phi_D), R)$ as the pdf of the 2D distance between the BS and the UAV located outside of the typical streets.*

$$\mathbb{P}_{LoS} = \int_{\phi_{D,1}}^{\phi_{D,2}} f_\Phi(\phi_D)d\phi_D \int_{\frac{x_0}{\cos(\phi_D)}}^{R} f_L(\ell_{2D})\Bigg[F_{H_B}\big(h_m^0(\ell_{2D},\phi_D)\big)\times \exp\left(-\lambda\int_{x_0}^{\ell_x}\Big[1-F_{H_B}\big(h_m^x(x,\ell_{2D},\phi_D)\big)\Big]dx - \lambda\int_{y_0}^{\ell_y}\Big[1-F_{H_B}\big(h_m^y(y,\ell_{2D},\phi_D)\big)\Big]dy\right)\Bigg]d\ell_{2D}. \quad (19)$$

*Proof.* According to the deployment geometry, the BS can be located either at the intersection of two perpendicular typical streets or on a typical street. In both cases, if the UAV projection onto the ground plane is placed on the typical street, the LoS path is not occluded. For all other UAV locations, there is a non-zero probability that the LoS path is blocked, $(1-\mathbb{P}_{\text{LoS}})$.

To determine $\mathbb{P}_{\text{LoS}}$, one needs to integrate (19) over all of the possible orientations and distances from the BS to the UAV located outside of the typical streets. Hence, to determine the area LoS probability, we have to provide $p_{\text{s}}$ together with the integration limits for the two considered BS locations. The integrands in (19) are given as

$$f_\Phi(\phi_{\text{D}}) = \frac{1}{\phi_{\text{D,2}}-\phi_{\text{D,1}}}, \qquad f_L(\ell_{\text{2D}}) = \frac{\cos(\phi_{\text{D}})}{R\cos(\phi_{\text{D}})-x_0}. \quad (20)$$

Let us first determine $p_{\text{s}}$ and the integration limits for the BS located at the intersection as depicted in Fig. 2(a). For the UAV that is distributed uniformly within the BS coverage area, the LoS AoD is also distributed uniformly in $(0, 2\pi)$. We then calculate the minimum $\phi_{\text{D,1}}$ and the maximum $\phi_{\text{D,2}}$ AoD for

This article has been accepted for publication in a future issue of this journal, but has not been fully edited. Content may change prior to final publication. Citation information: DOI 10.1109/TWC.2021.3075099, IEEE Transactions on Wireless Communications



the UAV projection onto the ground plane located outside of the typical street to establish

$$\phi_{\mathrm{D},1} = \arcsin(K_{\mathrm{h}} w_{\mathrm{h}}/R),\ \phi_{\mathrm{D},2} = \arccos(K_{\mathrm{v}} w_{\mathrm{v}}/R). \quad (21)$$

The probability of the UAV being placed on the typical street with BS, $p_{\mathrm{s}}$, is then available as a ratio of the street area to the total cell area, $\pi R^2$. To establish the typical street area, we calculate the segment area associated with the angle $\theta_{\mathrm{v},1}$ and the typical vertical street, see Fig. 2(a). The opposite segment area is obtained by using the angle $\theta_{\mathrm{v},2}$. We then subtract these areas from the circle area and arrive at the typical vertical street area.

The same approach is employed to characterize the area of the typical horizontal street. Accordingly, we add two typical street areas together and then subtract the common intersection area as it appears two times. We thus have

$$p_{\mathrm{s}} = 2 - \frac{\theta_{\mathrm{v},1} - \sin(\theta_{\mathrm{v},1})}{2\pi} - \frac{\theta_{\mathrm{v},2} - \sin(\theta_{\mathrm{v},2})}{2\pi} - \frac{w_{\mathrm{h}} w_{\mathrm{v}}}{\pi R^2} - \\ - \frac{\theta_{\mathrm{h},1} - \sin(\theta_{\mathrm{h},1})}{2\pi} - \frac{\theta_{\mathrm{h},2} - \sin(\theta_{\mathrm{h},2})}{2\pi}, \quad (22)$$

where the angles $\theta_{\mathrm{v},1}$, $\theta_{\mathrm{v},2}$, $\theta_{\mathrm{h},1}$, and $\theta_{\mathrm{h},2}$ are as in Fig. 2(a):

$$\theta_{\mathrm{v},1} = 2\arccos\left(\frac{K_{\mathrm{v}} w_{\mathrm{v}}}{R}\right),\ \theta_{\mathrm{h},1} = 2\arccos\left(\frac{K_{\mathrm{h}} w_{\mathrm{h}}}{R}\right), \\ \theta_{\mathrm{v},2} = 2\arccos\left(\frac{(1-K_{\mathrm{v}}) w_{\mathrm{v}}}{R}\right), \\ \theta_{\mathrm{h},2} = 2\arccos\left(\frac{(1-K_{\mathrm{h}}) w_{\mathrm{h}}}{R}\right). \quad (23)$$

For the BS located on the typical street, the approach is similar but has minor changes due to the deployment geometry, see Fig. 2(b). Particularly, the distances from point $T$ to the first endpoint of the $TR$ projection on the $X$- and $Y$-axis are

$$x_0 = K_{\mathrm{v}} w_{\mathrm{v}},\ y_0 = K_{\mathrm{v}} w_{\mathrm{v}} \tan(\phi_{\mathrm{D}}). \quad (24)$$

The minimum and the maximum angles for the location of the UAV residing outside the area of the typical street are given by

$$\phi_{\mathrm{D},1} = 0,\ \phi_{\mathrm{D},2} = \arccos(K_{\mathrm{v}} w_{\mathrm{v}}/R). \quad (25)$$

Finally, the probability that the UAV projection is placed on the street where the BS is positioned can be delivered by a ratio of the respective areas. Simplifying, we establish

$$p_{\mathrm{s}} = 1 - \frac{\theta_{\mathrm{v},1} - \sin(\theta_{\mathrm{v},1})}{2\pi} - \frac{\theta_{\mathrm{v},2} - \sin(\theta_{\mathrm{v},2})}{2\pi}, \quad (26)$$

where the angles to calculate the area segments are available as

$$\theta_{\mathrm{v},1} = 2\arccos\left(\frac{K_{\mathrm{v}} w_{\mathrm{v}}}{R}\right), \\ \theta_{\mathrm{v},2} = 2\arccos\left(\frac{(1-K_{\mathrm{v}}) w_{\mathrm{v}}}{R}\right). \quad (27)$$

After identifying the integration limits, we arrive at the integral form (19). Substituting (19) into (18), we conclude the proof for both cases. □

TABLE II
BASELINE SYSTEM PARAMETERS

| Parameter | Value |
|---|---|
| Height of BS, $h_{\mathrm{T}}$ | 10 m |
| Width of typical vertical street, $w_{\mathrm{v}}$ | 20 m |
| Width of typical horizontal street, $w_{\mathrm{h}}$ | 20 m |
| Coefficient $K_{\mathrm{v}}$ | 0.5 |

TABLE III
URBAN GRID GEOMETRY

| Type | Mean building height, $\mu_{\mathbf{H}}$ | Mean side width, $\mu_{\mathbf{b}}$ | Mean street width, $\mu_{\mathbf{s}}$ |
|---|---|---|---|
| Suburban | 10 m | 37 m | 10 m |
| Urban | 19 m | 45 m | 13 m |
| Dense urban | 25 m | 60 m | 20 m |
| Highrise urban | 63 m | 60 m | 20 m |

## V. NUMERICAL RESULTS

In this section, we evaluate the developed model numerically and illustrate the UAV LoS probability for several practical deployments. We start with assessing the accuracy and the applicability of our model by comparing its results with those obtained based on computer simulations. Then, we proceed by studying the impact of the system parameters and the urban deployment types on the UAV LoS probability. Finally, we compare the results of the proposed modeling to those discussed in the standards.

The default system parameters are summarized in Table II. To parametrize the scenario[2], we rely upon settings for an urban district as made available in [12] and [30]. Particularly, we consider four different urban grid types: (i) suburban, (ii) urban, (iii) dense urban, and (iv) highrise urban. We derive the relevant parameters of the considered urban deployments from the density of buildings, the fraction of land covered by them to the total area, as well as the variable for the height distribution provided by ITU-R [12], [30] to collect these in Table III.

### A. Accuracy and Applicability Limits

We begin by verifying the accuracy of the developed model and assessing its applicability limits. For this purpose, we develop a simulator that relaxes the following key assumption on the urban deployment as adopted in Section III: the probability that the LoS projection intersects a building block is always one. Recall that this assumption stems from the typical urban deployments, where the street width is usually much smaller than the block width.

In Fig. 3, we offer a comparison between the UAV LoS probability obtained with the developed mathematical model vs. computer simulations for a dense urban deployment (see Table III), Rayleigh distribution of the building heights $H_{\mathrm{B}} \sim \mathrm{Rayleigh}(20)$ as in [30], block and street mean widths ($\mu_{\mathrm{b}}$ and $\mu_{\mathrm{s}}$) of 60 m and 20 m, respectively. The simulations were conducted by employing the method of replications [34].

[2]The general form of the LoS probability in (7) can accept any building height distribution. Moreover, one can parametrize our model by using the statistical data of a particular city or district by extracting it from the database.

This article has been accepted for publication in a future issue of this journal, but has not been fully edited. Content may change prior to final publication. Citation information: DOI 10.1109/TWC.2021.3075099, IEEE Transactions on Wireless Communications



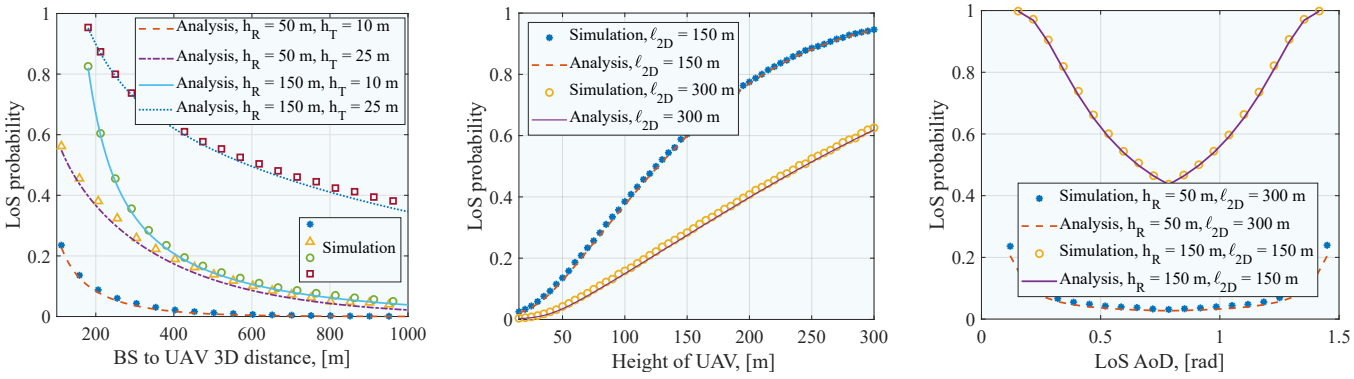


(a) As function of 3D distance (b) As function of UAV height (c) As function of LoS AoD

Fig. 3. LoS probability as function of UAV location in dense urban deployments. Building heights follow Rayleigh distribution $H_{\mathrm{B}} \sim \mathrm{Rayleigh}(20)$. BS is located in the center of intersection of two typical streets with the width of 20 m. LoS AoD $\phi_{\mathrm{D}}$ for subplots (a) and (b) is $30^o$.

First, in a single run, our modeler generates the considered deployment and then assesses the LoS path to the UAV located within the region at a certain distance, height, and angle with respect to the $X$-axis. A sequence of these runs forms statistically independent samples. Due to acceptable complexity of modeling the environment, we were able to carry out a sufficient number of experiments, such that the confidence intervals were always under $0.01$ of the respective absolute values for the level of significance set to $0.95$.

As a result, Fig. 3 demonstrates only point statistical estimates. As one may observe, the simulation output agrees tightly with the analytical results across a realistic range of the input parameters. The computational complexity of the simulations grows linearly as the density of building blocks increases. Specifically, the system-level modeling complexity is $O(N)$, whereas for the analytical derivations it remains constant at $O(1)$. Statistical LoS/nLoS probability models have proven themselves as computationally effective yet accurate tools [10]. Hence, we primarily resort to our developed analytical model for the purposes of this numerical analysis.

Observe that our assumption of LoS path always intersecting the block is actually close to reality where the block width is much larger than the street width as assumed in Fig. 3.

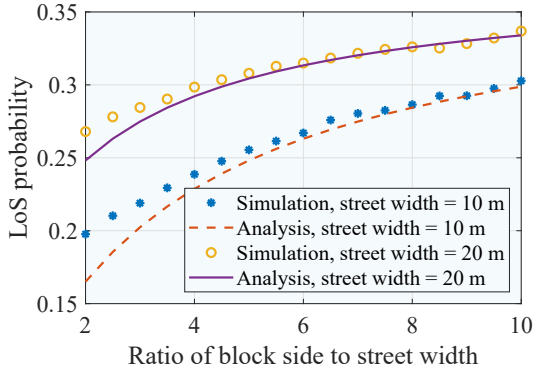


Fig. 4. Effects of the ratio of block side to street mean width on modeling accuracy. Building heights follow Rayleigh distribution $H_{\mathrm{B}} \sim \mathrm{Rayleigh}(20)$. BS is located in the center of intersection of two typical streets. UAV height is 150 m, 2D distance between BS and UAV is 300 m, LoS AoD $\phi_{\mathrm{D}}$ is $30^o$.

Let us now consider the response of our model to different ratios of block side to street mean widths as studied in Fig. 4 for a dense urban deployment, Rayleigh distribution ($H_{\mathrm{B}} \sim \mathrm{Rayleigh}(20)$) of the building heights, UAV altitude of 150 m, 300 m 2D distance to the UAV, and LoS AoD of $30^o$.

Analyzing the collected data, one may observe that the accuracy of the considered model heavily depends on the ratio between the block width and the street width. If the block width becomes larger than the street width, as in typical urban deployments, our formulation is more accurate in approximating the LoS probability. For the ratio of two and the street widths of 10 and 20 m, the difference between the simulation and the analysis is around 3% and 2%, respectively. After increasing the ratio further, this difference decreases. This behavior demonstrates the dominant effect of the block side width compared to the street width on the LoS probability analysis.

### B. UAV LoS Blockage Analysis

*1) Effects of UAV and BS Positions:* We continue by assessing the effects of the UAV and BS placement on the UAV LoS probability. We first address the impact of the UAV location with respect to the BS. Particularly, Fig. 3 illustrates the influence of the BS to UAV 3D distance, UAV height, BS height, and LoS AoD on the UAV LoS probability for the Rayleigh distribution ($H_{\mathrm{B}} \sim \mathrm{Rayleigh}(20)$) of the building heights. As our typical deployment, we choose dense urban layout characterized by the mean street width of 20 m and the side width of 60 m.

We consider the effect of 3D distance as displayed in Fig. 3(a) for the LoS AoD of $30^o$, BS height of 10 m, and two UAV flight heights, 50 and 150 m. As one may observe, the UAV LoS probability decreases exponentially with the growing distance from the BS. Further, the impact of the UAV height is of paramount importance. The difference in the absolute values of LoS probabilities between the two considered altitudes can reach $0.7$.

We then increase the BS height to 25 m as one of the typical heights for the Urban Macro scenarios specified by 3GPP [11]. We note that for the lower UAV height of 50 m, the BS height

This article has been accepted for publication in a future issue of this journal, but has not been fully edited. Content may change prior to final publication. Citation information: DOI 10.1109/TWC.2021.3075099, IEEE Transactions on Wireless Communications



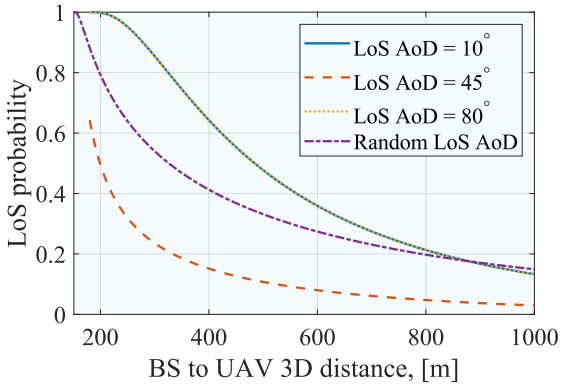


Fig. 5. Angle-dependent and -independent UAV LoS probability for dense urban deployment. Building heights follow Rayleigh distribution $H_{\mathrm{B}} \sim \mathrm{Rayleigh}(20)$. BS is located in the center of intersection of two typical streets with width of 20 m. UAV height is 150 m.

increase from 10 to 25 m, and the 2D separation distance of 100 m the LoS probability grows by 2.3 times. For the same set of parameters and the greater UAV height of 150 m, the BS height of 25 m yields the growth of the LoS probability by 1.1 times.

Fig. 3(b) details this aspect by presenting the UAV LoS probability across a wide range of UAV altitudes for two 2D distances between the UAV and the BS. As one may note, by increasing the UAV height up to 300 m and for the 2D distance of 150 m, the LoS probability may reach 0.95.

The orientation of the UAV with respect to the BS is also essential for the LoS probability assessment as confirmed by Fig. 3(c). As one may learn, the LoS probability for the UAV height of 150 m and the 2D distance of 150 m is around 1 for the LoS AoD close to 0 and $\pi/2$. At these LoS AoDs, the UAV is located sufficiently close to the typical street where the BS is deployed. Such a proximity reduces the number of buildings potentially occluding the LoS between the UAV and the BS, thus leading to higher LoS probability. It then gradually decreases and reaches its minimum at $\pi/4$ orientation of the LoS AoD, see Fig. 3(c).

We note that this behavior is an important property of realistic non-isotropic deployments that is not captured by the standard Poisson-like models, which implies that the LoS probability heavily depends on the UAV location with respect to its BS. This effect is further emphasized in Fig. 5, which shows the UAV LoS probability for different LoS AoDs as well as the area LoS probability (BS is located at the intersection) as a function of 3D distance between the BS and the UAV for the UAV height of 150 m. As one may see, the LoS probabilities for the LoS AoDs of $10^o$ and $80^o$ coincide due to equal intensity of points along the $X$- and $Y$-axes.

Furthermore, the area LoS probability may drastically deviate from the LoS probability for a particular LoS AoD, which accentuates the importance of the LoS AoD when evaluating the LoS probability for the UAVs. Regarding position-dependent UAV LoS probability, we conclude that the relative position of the UAV with respect to its BS largely affects the LoS probability even when the UAV height is much greater than the mean building height, which calls for a careful planning of UAV flight trajectories.

*2) Effects of Building Height Distribution:* As one may expect, the building height distribution produces a substantial impact on the UAV LoS probability. Most of the models proposed to date capture only the first moment of the building height by completely disregarding its higher moments as well as the form of the distribution itself. However, the architecture of urban districts may yield a considerable variation in the building heights.

In Fig. 6, we explore the impact of the building height distribution on the UAV LoS probability. To this aim, we evaluate the UAV LoS probability for a set of candidate building height distributions (uniform, gamma, Rayleigh, and exponential) as a function of its mean value for a constant variance of 33, see Fig. 6(a). In Fig. 6(b), we plot the LoS probability as a function of the standard deviation for a constant mean related to a certain district type (see Table III) and a gamma distribution of the building heights. Here, the 2D separation distance is 300 m, the LoS AoD is $30^o$, and the UAV height is 150 m.

As one may infer by analyzing the data in Fig. 6(a), the form of the distribution has a major effect on the UAV LoS probability. Particularly, up to the mean building height of 20 m, the results for all three distributions deviate in-

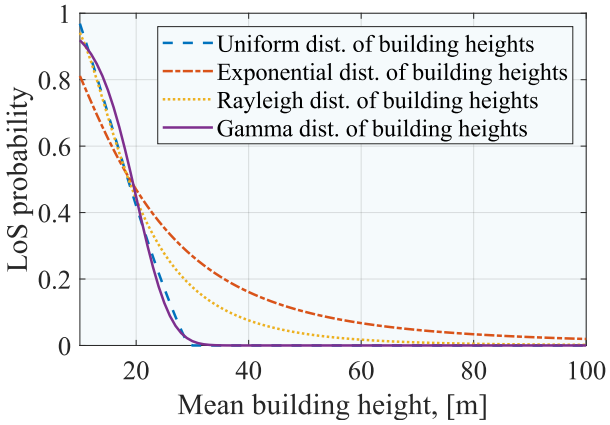


(a) Constant variance = 33

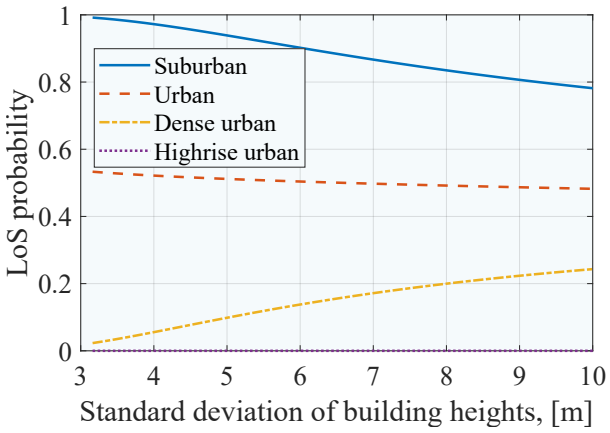


(b) Constant mean

Fig. 6. LoS probability as function of building height distribution for 2D separation distance of 300 m, LoS AoD of $30^o$, and UAV height of 150 m.

This article has been accepted for publication in a future issue of this journal, but has not been fully edited. Content may change prior to final publication. Citation information: DOI 10.1109/TWC.2021.3075099, IEEE Transactions on Wireless Communications



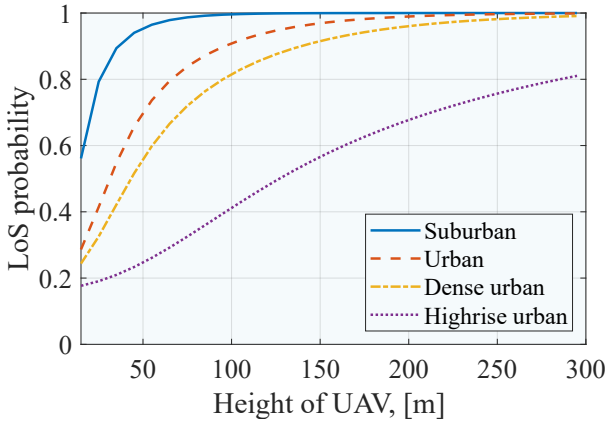


Fig. 7. Impact of urban deployment type on area LoS probability. BS coverage radius is 150 m and building height distribution is $H_{\mathrm{B}} \sim \text{Rayleigh}(\gamma)$.

significantly and remain within approximately 0.1 of each other. However, for greater average building heights of up to 60 m, which are typical for highrise urban deployments, the difference can become more substantial. A further increase in the mean building heights yields the LoS probability of close to 0, with almost no difference across various building height distributions.

Fig. 6(b) further illustrates the impact of the building height distribution as a function of the standard deviation, while keeping its mean related to a particular urban deployment as in Table III. Understanding the presented results, one may note that the difference is observable across the entire range of the standard deviations and for all the urban deployment types. Hence, we may conclude that for those layouts where the mean building height is under 20 m (e.g., suburban, urban, and dense urban), the models capturing the mean and the variance are sufficient for an accurate assessment of the UAV LoS probability.

For the deployments characterized by greater mean building heights (e.g., highrise urban), capturing the form of the height distribution is, however, essential. Regarding the effects of the building height distribution, we note that not only the first two moments but also the form of the distribution affect the UAV LoS probability, especially in the range [20 m,...,60 m] of the mean building heights. In what follows, we compare our proposed model with those standardized to date, which tend to disregard this crucial parameter.

*3) Effects of Urban Deployment Type:* We proceed with studying the effects of an urban deployment type on the UAV LoS probability by using the area LoS probability as specified in Proposition 2 for the scenario with the BS located at the intersection of two typical streets. Particularly, Fig. 7 demonstrates the considered parameter of interest as a function of the UAV height for the UAVs deployed uniformly within the BS coverage of 150 m. The building height distribution is assumed to be $H_{\mathrm{B}} \sim \text{Rayleigh}(\gamma)$, where $\gamma$ is equal to $\mu_H \sqrt{\frac{2}{\pi}}$. As one may observe, the area LoS probability is highly sensitive to the type of urban deployment since the absolute deviation may be up to 0.8.

As one may notice, for all of the deployments except for the highrise urban case the trend is exponential. In the case of a highrise urban deployment, the area LoS probability grows slower than exponential for the UAV heights under approximately 63 m. This effect is attributed to the relation between the mean UAV height and the mean building height. Particularly, whenever $\mu_{\mathrm{H}} \geq h_{\mathrm{R}}$, the rise is slower than exponential. Regarding the impact of urban deployments, we may deduce that in practice the minimum height of the UAV needs to be different for various layout options.

### C. Comparison with Standardized Models

We conclude with a comparison of our proposed LoS formulation against the presently standardized models to quantify the impact of more detailed parametrization. Fig. 8 demonstrates a comparison between the considered LoS probability model and the models specified in [11], [12] as functions of BS-to-UAV 2D distance in Fig. 8(a) and UAV height in Fig. 8(b). The standardized models were discussed earlier in subsection II-C, where (1) represents the ITU-R model while the 3GPP model is captured by (2).

We observe that the ITU-R LoS model completely disregards the features of spatial urban deployments by assuming

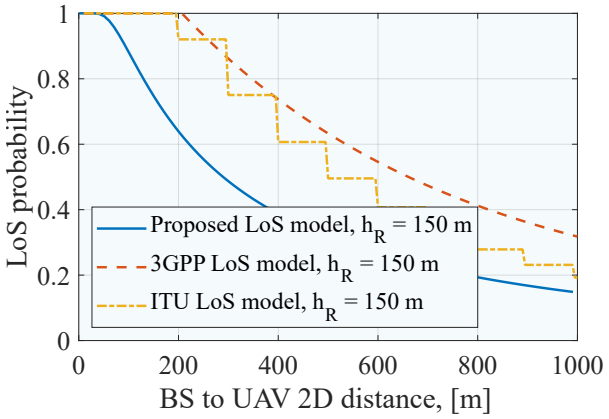


(a) As function of 2D distance

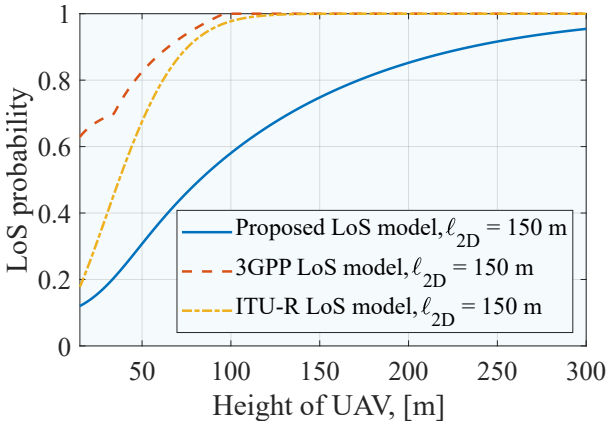


(b) As function of UAV height

Fig. 8. Area LoS probability as function of UAV location for three models: (i) proposed LoS model for dense urban deployment and BS located at the intersection of two streets, building height distribution is $H_{\mathrm{B}} \sim \text{Rayleigh}(20)$; (ii) 3GPP UMi street canyon LoS model (see 2); and (iii) ITU LoS model (see 1).

This article has been accepted for publication in a future issue of this journal, but has not been fully edited. Content may change prior to final publication. Citation information: DOI 10.1109/TWC.2021.3075099, IEEE Transactions on Wireless Communications



the building bases to be perpendicular to the LoS projection. Further, the 3GPP model does not specify the deployment parameters to characterize the LoS model. Hence, to provide a fair comparison between the formulations in question, Fig. 8 reports the area LoS probability for the dense urban deployment and the BS located at the intersection of two streets.

Analyzing the presented results, one may note that both ITU-R and 3GPP models capture the qualitative behavior of the UAV LoS probability since all three options lead to an exponential decrease for the parameter of interest in Fig. 8(a) under the growing 2D separation distance. However, both ITU-R and (especially) 3GPP formulations provide overly optimistic results for the practical separation distances. This is because the difference in terms of the absolute values can be up to $0.4$, which limits the use of these models for various urban grid deployments. One may also observe the stepwise behavior of the ITU-R formulation caused by a floor function in the model specification, which may complicate the use of this approach for analytical assessment.

Comparing the considered models with respect to the UAV height in Fig. 8(b), one may learn that both 3GPP and ITU-R options again drastically overestimate the actual UAV LoS probability. It is noted that both standardized formulations are much closer to each other than to our more exact model, where the difference may reach $0.4$. *We emphasize that a part of this discrepancy can be attributed to the fact that the 3GPP model does not capture the essential features of urban deployments, such as the distribution of building heights and does not specify the exact deployment parameters it employed.*

At the same time, the ITU-R model considers the deployment parameters as well as assumes a Rayleigh distribution of building heights but only accounts for a fixed number of buildings between the BS and its user. It also disregards the spatial distribution of buildings. All of these facts lead to a significant overestimation of the LoS probability by contrast to the proposed LoS probability model, which captures the essential features of urban deployments.

## VI. Conclusion and Future Work

In this work, we develop a model for the LoS probability evaluation on the BS-to-UAV link operating over mmWave frequency bands in 3D regular urban grid deployments as a function of building density as well as heights of the UAV, BS, and buildings. For a set of well-known building height distributions, closed-form expressions for the LoS probability are provided. In contrast to similar past formulations, our model allows to account for different building height distributions, spatial link orientations, as well as various deployment parameters, such as density of buildings. As a result, the flexibility of our formulation permits to study dissimilar urban deployment types, including suburban, urban, dense urban, and highrise urban layouts. We also note that the developed model can be suitable for systems other than mmWave, assuming an optical LoS for modeling purposes.

Our numerical results demonstrate that the UAV LoS probability heavily depends on the BS-to-UAV link orientation with respect to the non-isotropic deployment grid. For instance, the BS-to-UAV LoS AoD of $\pi/4$ makes the LoS probability drop by almost a half as compared to the LoS AoD equal to $\pi/2$. This implies that the choice of the UAV flight trajectory is crucial for maintaining high LoS probability and thus reliable connectivity between the UAV and the BS. Further, our study accentuates the importance of accounting for the building height distribution as it has a profound impact on the LoS probability. By comparing our model with the standard ITU and 3GPP alternatives, we argue that they both provide extremely coarse approximations for the UAV LoS probability as they do not capture the essential features of urban grid deployments, while our approach can be more accurate and applicable to various deployments.

To ensure reliable UAV support, it is imperative to conduct a thorough analysis of the underlying network deployment. The developed LoS probability formulation can thus become an integral part of comprehensive system-level modeling frameworks. The latter can merge the evaluated LoS probability values with the UAV-to-ground propagation model [35], [36] by additionally accounting for the transmit power, antenna gains at the BS and UAV sides, possible beam misalignment, as well as blockage-induced attenuation. Since conventional cellular deployments employ downtilted antennas, the existence of an unobstructed LoS path between the UAV and the BS does not however guarantee that communication is feasible [37]. To capture this situation, one needs to account for the antenna downtilt and evaluate the maximum user height to be supported by the BS main lobe at a given distance as well as the probability of having side lobes available. These results may project, e.g., the required BS density to minimize the link interruption times between the UAV and the terrestrial network infrastructure.

## Appendix A
## Consideration of Rooftop BSs

Reliable support of UAVs in early-stage 5G deployments may require provisional network nodes mounted on, e.g., rooftops of the buildings. The model developed in this work can capture this important case as demonstrated below.

When the height of a rooftop-mounted BS is known in advance, one may directly apply our formulation by setting the appropriate height in (7). Alternatively, one may assume random heights of rooftop-mounted BSs. To account for this case, we need to modify (7) as

$$\mathbb{P}_{\text{LoS}}(\ell_{\text{2D}},\phi_{\text{D}}) = \int_0^{\infty} \Bigg( F_{H_{\text{B}}}\big(h^0_{\text{m}}(\ell_{\text{2D}},\phi_{\text{D}},z)\big)\times \exp\Bigg(-\lambda \int_{x_0}^{\ell_{\text{x}}} \Big[1-F_{H_{\text{B}}}\big(h^x_{\text{m}}(x,z,\ell_{\text{2D}},\phi_{\text{D}})\big)\Big]\mathrm{d}x - \lambda \int_{y_0}^{\ell_{\text{y}}} \Big[1-F_{H_{\text{B}}}\big(h^y_{\text{m}}(y,z,\ell_{\text{2D}},\phi_{\text{D}})\big)\Big]\mathrm{d}y\Bigg) f_{H_{\text{B}}}(z)\mathrm{d}z\Bigg), \quad (28)$$

where $f_{H_{\text{B}}}$ is the pdf of the building heights and $z$ is the height of the rooftop BS.

## REFERENCES


[1] Z. Xiao, P. Xia, and X. Xia, "Enabling UAV cellular with millimeter-wave communication: potentials and approaches," *IEEE Communications Magazine*, vol. 54, no. 5, pp. 66–73, May 2016.

[2] Y. Zeng, J. Lyu, and R. Zhang, "Cellular-connected UAV: Potential, challenges, and promising technologies," *IEEE Wireless Communications*, vol. 26, no. 1, pp. 120–127, February 2019.

[3] 3GPP, "3GPP SA6 accelerates work on new verticals!" 3GPP available at: https://www.3gpp.org/news-events/2045-sa6_verticals, June 2019.

[4] ——, "Enhancement for unmanned aerial vehicles; stage 1 (Release 17)," 3GPP TR 22.829 V17.0.0, September 2019.

[5] W. Xia, M. Polese, M. Mezzavilla, G. Loianno, S. Rangan, and M. Zorzi, "Millimeter wave remote UAV control and communications for public safety scenarios," in *2019 16th Annual IEEE International Conference on Sensing, Communication, and Networking (SECON)*, 2019, pp. 1–7.

[6] A. A. Khuwaja, Y. Chen, N. Zhao, M. Alouini, and P. Dobbins, "A survey of channel modeling for UAV communications," *IEEE Communications Surveys & Tutorials*, vol. 20, no. 4, pp. 2804–2821, Fourthquarter 2018.

[7] M. Mozaffari, W. Saad, M. Bennis, Y. Nam, and M. Debbah, "A tutorial on UAVs for wireless networks: Applications, challenges, and open problems," *IEEE Communications Surveys & Tutorials*, vol. 21, no. 3, pp. 2334–2360, Thirdquarter 2019.

[8] H. Shakhatreh, A. H. Sawalmeh, A. Al-Fuqaha, Z. Dou, E. Almaita, I. Khalil, N. S. Othman, A. Khreishah, and M. Guizani, "Unmanned aerial vehicles (UAVs): A survey on civil applications and key research challenges," *IEEE Access*, vol. 7, pp. 48 572–48 634, 2019.

[9] W. Khawaja, I. Guvenc, D. W. Matolak, U. Fiebig, and N. Schneckenburger, "A survey of air-to-ground propagation channel modeling for unmanned aerial vehicles," *IEEE Communications Surveys & Tutorials*, vol. 21, no. 3, pp. 2361–2391, thirdquarter 2019.

[10] T. S. Rappaport, Y. Xing, G. R. MacCartney, A. F. Molisch, E. Mellios, and J. Zhang, "Overview of millimeter wave communications for fifth-generation (5G) wireless networks-with a focus on propagation models," *IEEE Transactions on Antennas and Propagation*, vol. 65, no. 12, pp. 6213–6230, 2017.

[11] 3GPP, "Study on enhanced LTE support for aerial vehicles, (Release 15)," TR 36.777 V15.0.0, January 2018.

[12] ITU-R, "Propagation data and prediction methods required for the design of terrestrial broadband radio access systems operating in a frequency range from 3 to 60 GHz," Rec. ITU-R P.1410, February 2012.

[13] ——, "Technical feasibility of IMT in bands above 6 GHz," Report ITU-R M.2376-0, July 2015.

[14] T. Bai and R. W. Heath, "Analysis of self-body blocking effects in millimeter wave cellular networks," in *48th Asilomar Conference on Signals, Systems and Computers*, 2014, pp. 1921–1925.

[15] M. Gapeyenko, A. Samuylov, M. Gerasimenko, D. Moltchanov, S. Singh, E. Aryafar, S. Yeh, N. Himayat, S. Andreev, and Y. Koucheryavy, "Analysis of human-body blockage in urban millimeter-wave cellular communications," in *IEEE International Conference on Communications (ICC)*, 2016, pp. 1–7.

[16] R. Kovalchukov, D. Moltchanov, A. Samuylov, A. Ometov, S. Andreev, Y. Koucheryavy, and K. Samouylov, "Evaluating SIR in 3D millimeter-wave deployments: Direct modeling and feasible approximations," *IEEE Transactions on Wireless Communications*, vol. 18, no. 2, pp. 879–896, February 2019.

[17] M. Comisso and F. Babich, "Coverage analysis for 2D/3D millimeter wave peer-to-peer networks," *IEEE Transactions on Wireless Communications*, vol. 18, no. 7, pp. 3613–3627, 2019.

[18] J. G. Andrews, T. Bai, M. N. Kulkarni, A. Alkhateeb, A. K. Gupta, and R. W. Heath, "Modeling and analyzing millimeter wave cellular systems," *IEEE Transactions on Communications*, vol. 65, no. 1, pp. 403–430, January 2017.

[19] E. Ogawa and A. Satoh, "Propagation path visibility estimation for radio local distribution systems in built-up areas," *IEEE Transactions on Communications*, vol. 34, no. 7, pp. 721–724, July 1986.

[20] S. Saunders, C. Tzaras, and B. Evans, "Physical–statistical methods for determining state transition probabilities in mobile–satellite channel models," *International Journal of Satellite Communications*, vol. 19, no. 3, pp. 207–222, May 2001.

[21] Q. Feng, E. K. Tameh, A. R. Nix, and J. McGeehan, "WLCp2-06: Modelling the likelihood of line-of-sight for air-to-ground radio propagation in urban environments," in *IEEE Global Communications Conference*, November 2006, pp. 1–5.

[22] T. Bai, R. Vaze, and R. W. Heath Jr., "Analysis of blockage effects on urban cellular networks," *IEEE Transactions on Wireless Communications*, vol. 13, no. 9, pp. 5070–5083, September 2014.

[23] K. Han, K. Huang, and R. W. Heath, "Connectivity and blockage effects in millimeter-wave air-to-everything networks," *IEEE Wireless Communications Letters*, vol. 8, no. 2, pp. 388–391, April 2019.

[24] T. Bai and R. W. Heath, "Coverage and rate analysis for millimeter-wave cellular networks," *IEEE Transactions on Wireless Communications*, vol. 14, no. 2, pp. 1100–1114, February 2015.

[25] X. Liu, J. Xu, and H. Tang, "Analysis of frequency-dependent line-of-sight probability in 3-D environment," *IEEE Communications Letters*, vol. 22, no. 8, pp. 1732–1735, 2018.

[26] F. Baccelli and X. Zhang, "A correlated shadowing model for urban wireless networks," in *2015 IEEE Conference on Computer Communications (INFOCOM)*, April 2015, pp. 801–809.

[27] A. Colpaert, E. Vinogradov, and S. Pollin, "Aerial coverage analysis of cellular systems at LTE and mmWave frequencies using 3D city models," *Sensors*, vol. 18, no. 12, 2018.

[28] J. Järveläinen, S. L. H. Nguyen, K. Haneda, R. Naderpour, and U. T. Virk, "Evaluation of millimeter-wave line-of-sight probability with point cloud data," *IEEE Wireless Communications Letters*, vol. 5, no. 3, pp. 228–231, 2016.

[29] M. K. Samimi, T. S. Rappaport, and G. R. MacCartney, "Probabilistic omnidirectional path loss models for millimeter-wave outdoor communications," *IEEE Wireless Communications Letters*, vol. 4, no. 4, pp. 357–360, 2015.

[30] A. Al-Hourani, S. Kandeepan, and S. Lardner, "Optimal LAP altitude for maximum coverage," *IEEE Wireless Communications Letters*, vol. 3, no. 6, pp. 569–572, December 2014.

[31] D. E. Berraki, S. M. D. Armour, and A. R. Nix, "Benefits of the sparsity of mmwave outdoor spatial channels for beamforming and interference cancellation," *Physical Communication*, vol. 27, pp. 170–180, April 2018.

[32] D. R. Cox and V. Isham, *Point processes*. CRC Press, 1980, vol. 12.

[33] L. Chen, J. Hang, M. Sandberg, L. Claesson, S. Di Sabatino, and H. Wingo, "The impacts of building height variations and building packing densities on flow adjustment and city breathability in idealized urban models," *Building and Environment*, vol. 118, pp. 344–361, June 2017.

[34] R. Jain, *The art of computer systems performance analysis: techniques for experimental design, measurement, simulation, and modeling*. John Wiley & Sons, 1990.

[35] M. Polese, L. Bertizzolo, L. Bonati, A. Gosain, and T. Melodia, "An experimental mmwave channel model for UAV-to-UAV communications," in *4th ACM Workshop on Millimeter-Wave Networks and Sensing Systems (mmNets'20)*, 2020.

[36] M. T. Dabiri, H. Safi, S. Parsaeefard, and W. Saad, "Analytical channel models for millimeter wave UAV networks under hovering fluctuations," *IEEE Transactions on Wireless Communications*, vol. 19, no. 4, pp. 2868–2883, 2020.

[37] G. Geraci, A. Garcia-Rodriguez, L. Galati Giordano, D. López-Pérez, and E. Björnson, "Understanding UAV cellular communications: From existing networks to massive MIMO," *IEEE Access*, vol. 6, pp. 67 853–67 865, 2018.


**Margarita Gapeyenko** is a Ph.D. candidate at the Unit of Electrical Engineering at Tampere University, Finland. She earned M.Sc. degree in Telecommunication Engineering from University of Vaasa, Finland, in 2014, and B.Sc. degree in Radio Engineering, Electronics, and Telecommunications from KSTU, Kazakhstan, in 2012. Her research interests include mathematical analysis, performance evaluation, and optimization methods for mmWave networks, UAV communications, and (beyond-)5G heterogeneous systems.

**Dmitri Moltchanov** received the M.Sc. and Cand.Sc. degrees from St. Petersburg State University of Telecommunications, Russia, in 2000 and 2003, respectively, and the Ph.D. degree from Tampere University of Technology in 2006. Currently, he is a University Lecturer with the Faculty of Information Technology and Communication Sciences, Tampere University, Finland. He has (co-)authored over 150 publications. His current research interests include 5G/5G+ systems, ultra-reliable low-latency service, industrial IoT applications, mission-critical V2V/V2X systems, and blockchain technologies.

**Sergey Andreev** (SM'17) is an associate professor of communications engineering and Academy Research Fellow at Tampere University, Finland. He has been a Visiting Senior Research Fellow with King's College London, UK (2018-20) and a Visiting Postdoc with University of California, Los Angeles, US (2016-17). He received his Ph.D. (2012) from TUT as well as his Specialist (2006), Cand.Sc. (2009), and Dr.Habil. (2019) degrees from SUAI. He is lead series editor of the IoT Series (2018-) for IEEE Communications Magazine and served as editor for IEEE Wireless Communications Letters (2017-19). He (co-)authored more than 200 published research works on intelligent IoT, mobile communications, and heterogeneous networking.

**Robert W. Heath Jr.** (S'96 - M'01 - SM'06 - F'11) received the B.S. and M.S. degrees from the University of Virginia, Charlottesville, VA, in 1996 and 1997 respectively, and the Ph.D. from Stanford University, Stanford, CA, in 2002, all in electrical engineering. From 1998 to 2001, he was a Senior Member of the Technical Staff then a Senior Consultant at Iospan Wireless Inc, San Jose, CA where he worked on the design and implementation of the physical and link layers of the first commercial MIMO-OFDM communication system. From 2002-2020 he was with The University of Texas at Austin, most recently as Cockrell Family Regents Chair in Engineering and Director of UT SAVES. He is presently a Distinguished Professor at North Carolina State University. He is also President and CEO of MIMO Wireless Inc. He authored "Introduction to Wireless Digital Communication" (Prentice Hall, 2017) and "Digital Wireless Communication: Physical Layer Exploration Lab Using the NI USRP" (National Technology and Science Press, 2012), and co-authored "Millimeter Wave Wireless Communications" (Prentice Hall, 2014) and "Foundations of MIMO Communication" (Cambridge University Press, 2018).

Dr. Heath has been a co-author of a number award winning conference and journal papers including recently the 2016 IEEE Communications Society Fred W. Ellersick Prize, the 2016 IEEE Communications and Information Theory Societies Joint Paper Award, the 2017 Marconi Prize Paper Award, the 2019 IEEE Communications Society Stephen O. Rice Prize, and the 2020 IEEE Signal Processing Society Overview Paper Award. He received the 2017 EURASIP Technical Achievement award and the 2019 IEEE Kiyo Tomiyasu Award. In 2017, he was selected as a Fellow of the National Academy of Inventors. He is a member-at-large on the IEEE Communications Society Board-of-Governors (2020-2022) and is a past member-at-large on the IEEE Signal Processing Society Board-of-Governors (2016-2018). He was Editor-in-Chief of IEEE Signal Processing Magazine from 2018-2020. He is also a licensed Amateur Radio Operator, a Private Pilot, a registered Professional Engineer in Texas.